SCIENTIFIC REPORTS

OPEN

SUBJECT AREAS:
SUPERCONDUCTING PROPERTIES AND MATERIALS
SUPERCONDUCTORS
GEOMAGNETISM

Received
29 October 2013

Accepted
4 December 2013

Published
14 January 2014

Correspondence and requests for materials should be addressed to C.Q.J. (Jin@iphy.ac.cn)

Magnetic and structural transitions of $SrFe_2As_2$ at high pressure and low temperature

J. J. Wu[1,2], J. F. Lin[2], X. C. Wang[1], Q. Q. Liu[1], J. L. Zhu[1], Y. M. Xiao[3], P. Chow[3] & C. Q. Jin[1]

[1]Beijing National Laboratory for Condensed Matter Physics and Institute of Physics, Chinese Academy of Sciences, Beijing 100190, China, [2]Department of Geological Sciences, Jackson School of Geosciences, The University of Texas at Austin, TX 78712, USA, [3]HPCAT, Carnegie Institution of Washington, Advanced Photon Source, Argonne National Laboratory, Argonne, IL 60439, USA.

One of key issues in studying iron based superconductors is to understand how the magnetic phase of the parent compounds evolves. Here we report the systematic investigation of paramagnetic to antiferromagnetic and tetragonal to orthorhombic structural transitions of "122" $SrFe_2As_2$ parent compound using combined high resolution synchrotron Mössbauer spectroscopy and x-ray diffraction techniques in a cryogenically cooled high pressure diamond anvil cell. It is found that although the two transitions are coupled at 205 K at ambient pressure, they are concurrently suppressed to much lower temperatures near a quantum critical pressure of approximately 4.8 GPa where the antiferromagnetic state transforms into bulk superconducting state. Our results indicate that the lattice distortions and magnetism jointly play a critical role in inducing superconductivity in iron based compounds.

The recent discovery of superconductivity in iron pnictide compounds[1] has drawn significant attention in studying the unconventional superconductivity containing magnetic elements. Following the first report on the superconductivity in "1111" RFeAsO system, a number of pnictide families have been reported including "122" $AeFe_2As_2$ (Ae = Ca, Sr, Ba), "111" AFePn (A: Li, Na, Pn: As, P), and "11" FeSe types[2–4]. The parent compounds of the iron pnictide superconductors contain FeAs tetrahedral layers and exhibit a tetragonal to orthorhombic structural transition as well as a paramagnetic (PM) to antiferromagnetic (AFM) transition[5,6]. The AFM orthorhombic phase has been shown to be the parent phase of the pnictide superconductor forming the spin density wave (SDW) state in which superconductivity can be induced by suppressing the SDW state via chemical doping or applied pressure[7,8]. The structural and magnetic phase transitions of the pnictide parent compounds have been shown to play an important role in inducing superconductivity[9]. For example, previous studies have indicated that "122" $SrFe_2As_2$ compound undergoes the structural and magnetic transitions simultaneously at T_S = 205 K at ambient pressure[10,11], while its superconductivity (SC) occurs once the SDW state is suppressed at high pressures[12]. On the other hand, chemical substitutions with electron or hole doping have been shown to suppress the AFM state of $SrFe_2As_2$, resulting in the occurrence of superconductivity even at ambient pressure[13,14]. The correlation between the suppression of the long-range magnetic ordering and the simultaneous formation of the SC state indicates that the spin fluctuation of the Fe moments plays a key role in establishing the superconductive state. Compared to chemical doping where disorders can be inevitably introduced[15,16], applied pressure introduces less lattice disorders than chemical doping, and has been shown to be an effective tool in deciphering the intrinsic superconducting behaviors in Fe-based superconductors[17,18]. Indeed, applied pressure not only increases the T_C in the $LaFeAs(O_{1-x}F_x)$, FeSe, AFePn (A: Li, Na, Pn: As, P) system[19–23], but it also induces superconductivity in the parent "122" compounds[24–27]. Superconductivity with high T_C up to 12 K appears at pressures between 0.23 and 0.86 GPa in $CaFe_2As_2$[27]. Similarly, pressure-induced superconductivity has been reported for $BaFe_2As_2$ and $SrFe_2As_2$ at approximately 3.0 GPa and 3.6 GPa, respectively[24,28]. Since the magnetic transition is strongly coupled with the structural distortion in the $SrFe_2As_2$ system at ambient pressure, studying its magnetic ordering, structural distortions, and superconductivity at high pressures and low temperatures under controlled hydrostatic conditions can provide valuable insight into intrinsic underlying mechanism for the origin of superconductivity in the system. Here we have investigated the magnetic and structural transitions of $SrFe_2As_2$ using synchrotron Mössbauer spectoscopy (SMS) and x-ray diffraction (XRD) in a cryogenically-cooled high-pressure diamond anvil cell (DAC) having a relatively hydrostatic Ne pressure medium. Our results show that the magnetic and structural transitions of $SrFe_2As_2$ remain strongly coupled at extreme pressure-temperature

environments. This sheds new light on the interplay of the lattice distortions and magnetism in the origin of superconductivity in the iron-based superconductors at high pressures and low temperatures.

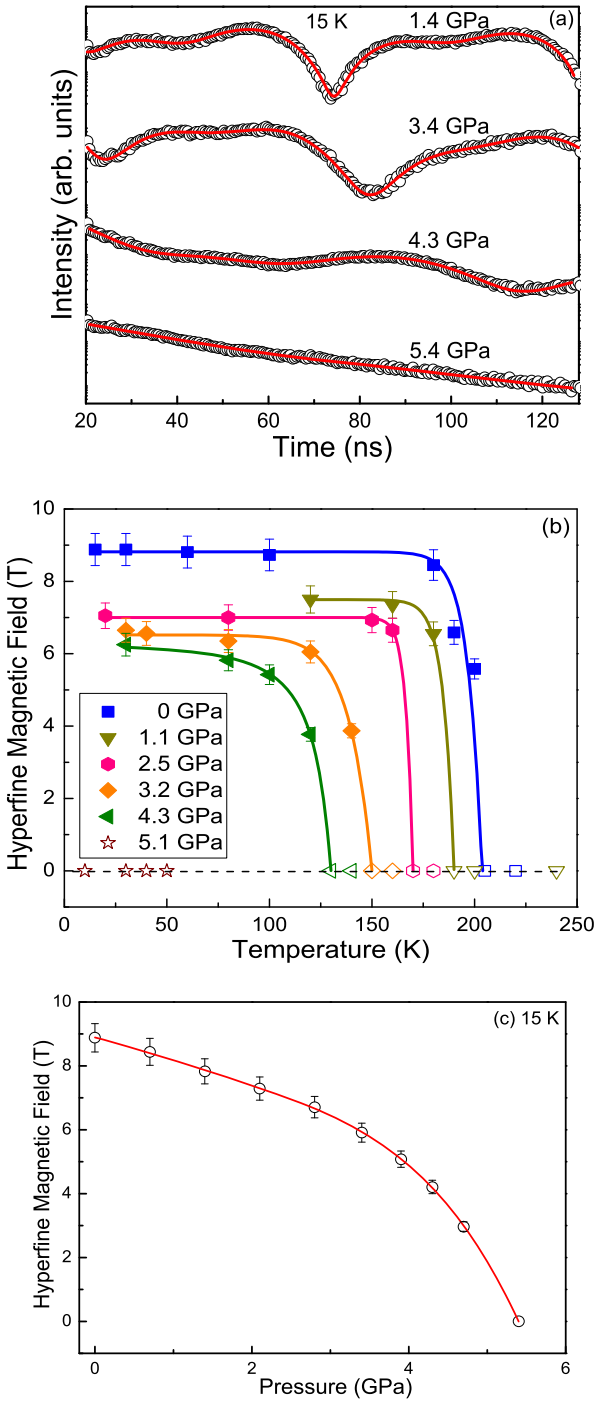

Figure 1 | (a) Representative pressure dependent SMS spectra of $SrFe_2As_2$ at 15 K in Ne medium. Open circles: experimental data; red solid lines: modeled spectra using CONUSS program. Quantum beats in the spectra represent the occurrence of the magnetic field and hence the AFM state, whereas the absence of the beats (flat spectral feature) is indicative of the PM state. (b) Derived hyperfine magnetic fields of the AFM $SrFe_2As_2$ as a function of temperature at representative high pressures. Appearance and disappearance of the magnetic fields are used to construct the magnetic PM-AFM transition as a function of *P*-*T*. Filled symbol: AFM state; open symbol: PM state. (c) Derived hyperfine magnetic fields of $SrFe_2As_2$ as a function pressure at 15 K.

Results

SMS spectra were collected up to 5.4 GPa and temperatures as low as 15 K, while XRD patterns were measured up to 8.2 GPa and 13 K (Figs. 1, 2). Fig. 1(a) shows representative pressure-dependent ^{57}Fe SMS spectra of $SrFe_2As_2$ at 15 K. At 1.4 GPa and 15 K, the drastic appearance of quantum beats manifests the splitting of ^{57}Fe nuclear level through hyperfine interaction, showing the AFM state. As pressure was increased to 4.3 GPa, the SMS spectrum changed significantly with the disappearance of the quantum beats, indicating that the magnetic phase had been suppressed via applied pressure at 15 K while the PM state started to appear. Since the spectrum could not be reasonably fitted using only paramagnetic or magnetic phases, both paramagnetic and magnetic phases were used to model the SMS spectrum at 4.3 GPa. Analyses of the modeled results showed that the magnetic phase accounts for approximately 42 vol.% of the two phases. At a higher pressure of approximately 5.4 GPa, the ^{57}Fe nuclear level is characterized by flat spectral features without any splitting quantum beats, indicating the sole existence of the PM state with the completely suppressed magnetism by pressure. The derived hyperfine parameters show an abrupt increase in the strength of the magnetic fields as a function of temperature at a given pressure (Fig. 1(b)). For example, at 2.5 GPa the hyperfine magnetic field

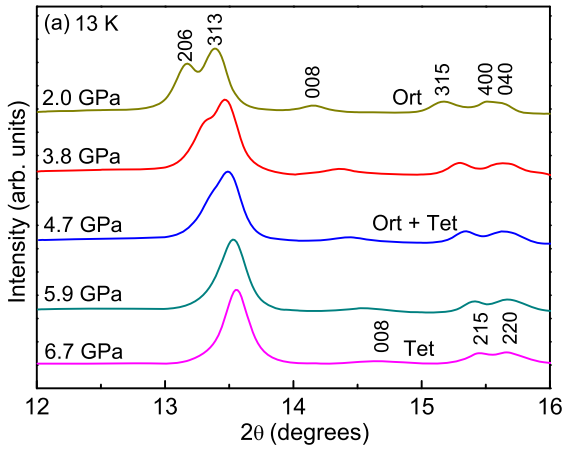

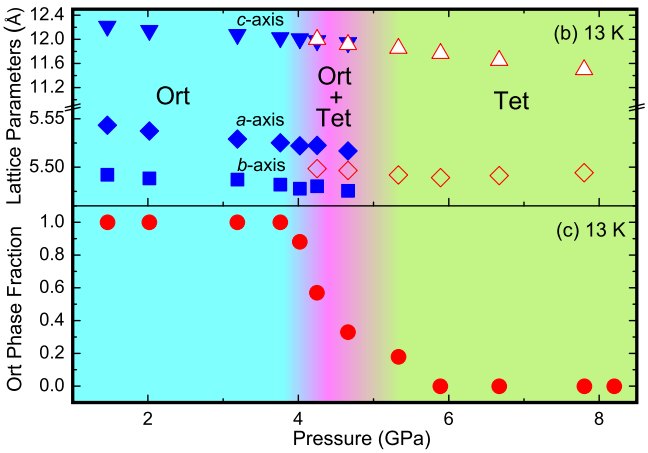

Figure 2 | (a) Representative synchrotron angle-dispersive x-ray diffraction of $SrFe_2As_2$ as a function of pressure at 13 K. Splitting of the 220 reflection to 400/040 is indicative of the tetragonal to orthorhombic transition at high pressures. Ort: orthorhombic phase; Tet: tetragonal phase. At 4.7 GPa, the orthorhombic and tetragonal phases coexist at 13 K. (b) Variation of lattice parameters with pressure at 13 K. (c) Volume fraction of the orthorhombic phase as a function of pressure at 13 K.

jumped to 6.7 T from zero as temperature was decreased to 160 K and then remains almost constant, indicating a PM to AFM transition. As pressure increases (Fig. 1(b)), the hyperfine magnetic field decreases and the magnetic transition region slightly broadens, implying suppressed magnetism by applied pressure; magnetism was totally suppressed at 5.1 GPa at each given low temperature as shown in Fig. 1(c).

In order to clarify the relationship between the structural and magnetic transitions, we have also performed XRD experiments under high pressures and low temperatures (Figs. 2). Analyses of the high-pressure XRD spectra showed that the (220) reflection of the tetragonal phase splits to (400) and (040) reflections that are characteristic of the tetragonal to orthorhombic structural transition in $SrFe_2As_2$ with decreasing temperature at a given pressure[11]. Similar to the magnetic transition, this structural transition is strongly suppressed by pressure (Fig. 2(a)). At a constant temperature of 13 K, derived lattices parameters in Fig. 2(b) show the existence of the orthorhombic phase (space group: *Fmmm*) below 4 GPa and the tetragonal phase (space group: I4/mmm) above 6 GPa, respectively, whereas there is a P-T region between 4 GPa and 6 GPa, in which the tetragonal and orthorhombic phases coexist. With increasing pressure, the orthorhombic phase observed in the region is suppressed while the abundance of the tetragonal phase is enhanced (Fig. 2(c)).

Combining our synchrotron SMS and XRD results (Figs. 1–2) with literature high T_c studies, we have constructed the structural, magnetic, and superconducting phase diagram of $SrFe_2As_2$ under high pressures and low temperatures (Fig. 3). The magnetic transition temperature (T_N) was defined as the mid-point between the first appearance of the hyperfine magnetic field and the last appearance of the paramagnetic phase, while the structural transition temperature (T_S) was defined as the mid-point from the pure tetragonal to the pure orthorhombic structural phase transition; for the co-existence of the tetragonal and orthorhombic phases at 13 K, the T_S is defined as the point of disappearance for the orthorhombic phase. At ambient pressure, previous studies showed that the structural transition concurs with the magnetic transition[10,11]. Our results here further show that, within experimental uncertainties, these two transitions are strongly coupled at high pressures and low temperatures (Fig. 3), except the P-T region overlap starting with the T_c dome where an extended P-T region of the two-phase coexistence was observed (see further details in Discussions). These transition temperatures decrease with increasing pressures up to approximately 4.6 GPa, but are drastically suppressed to zero at a quantum critical pressure (P_C) of 4.8 GPa.

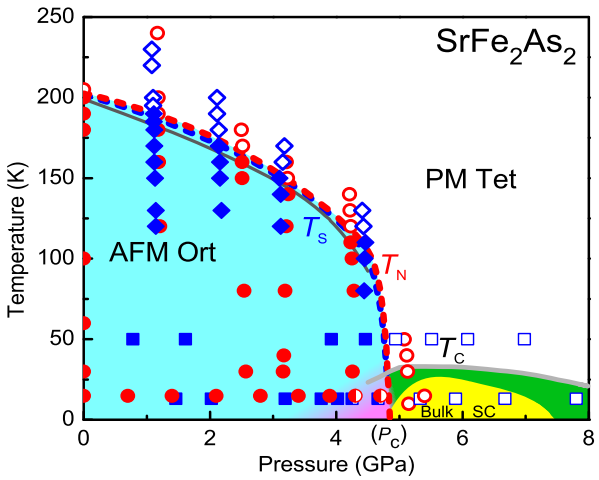

Figure 3 | Magnetic and structural transition diagram of $SrFe_2As_2$ at high pressures and low temperatures. XRD data: blue diamond symbols (λ = 0.4047 Å) and blue square symbols (λ = 0.3737 Å); SMS data: red circle symbols. T_S (blue dash line) and T_N (red dash line) are extracted from analyses of the data in order to define the structural and magnetic transition conditions. The superconducting transition temperature T_C with grey solid line for filamentary SC, as well as T_S with darker grey solid line for the structural transition is taken from Ref. 25 using single crystals in a cubic anvil having glycerin pressure medium, that were similar to our experimental conditions. A quantum critical phase transition at a P_c of 4.8 GPa is suggested. Tet: tetragonal structure; Ort: orthorhombic structure; AFM: antiferromagnetic; PM: paramagnetic. The half-filled red circles represent for the coexistence of PM and AFM phases, while the half-filled blue squares represent for the coexistence of Ort and Tet phases. The filled purple region represents for the coexistence of filamentary superconductivity, AFM Ort and PM Tet phases. Pressure uncertainties are smaller to the symbols, whereas temperature uncertainties are less than 5 K.

Discussions

As discussed in the previous studies of the "122" system, differential stress can strongly affect the critical pressure in the $BaFe_2As_2$ and $SrFe_2As_2$ compounds[29–31]. In order to draw a more direct, meaningful comparison with literature results, our structural and magnetic results are plotted on top of the superconducting transition from Ref.[25], which reported electrical resistivity and ac magnetic susceptibility measurements using a relatively hydrostatic glycerin medium that is similar in hydrostaticity to Ne medium used in our experiments. Comparisons of these results show that filamentary superconductivity with zero resistivity emerges with the occurrence of the tetragonal phase co-existing with the orthorhombic phase in the AFM state at around 4.2 GPa and 13 K. Our results also imply that filamentary superconductivity can only coexist with the partial magnetism in the mixed tetragonal and orthorhombic region in the $SrFe_2As_2$ at temperatures below 28 K and pressures between 4.2 and 4.8 GPa as shown in the filled purple region in Fig. 3. Furthermore, bulk superconductivity, as observed by an anomaly in the field cooling (FC) magnetic susceptibility, only appears in the P-T region with the tetragonal phase in the PM state, where the T_S and T_N transitions are fully suppressed. Based on both diffraction and Mössbauer results, the volume fraction of the AFM orthorhombic phase as a function of pressure appears to be inversely proportional to the high T_c (Figs. 2 and 3), further supporting the notion that the superconductivity is partially suppressed by the existence of magnetism in the AFM orthorhombic phase. Thus we assume the presence of an AFM quantum critical point (QCP) near the AFM phase boundary. Previous NMR experiments indicate an antiferromagnetic fluctuation associated with QCP has strong correlation with the high-T_c superconductivity in chemically-doped $BaFe_2As_2$ compounds[32,33]. These results indicate that the QCP is likely to connect with the superconductivity in the iron based compound.

Methods

Single-crystal $SrFe_2As_2$ samples with 20 at.% ^{57}Fe enrichment were grown using the FeAs self-flux method[34]. XRD analyses of the synthesized samples showed lattice parameters of a = 3.9234(3) Å and c = 12.371(2) Å at ambient conditions. A sample measuring 15 μm thick and 70 μm big was loaded into a symmetric DAC using Ne as the pressure medium, together with three ruby spheres for pressure calibration at low temperatures. The pressure of the sample chamber was controlled using a membrane diaphragm. A helium flow cold-finger cryostat was used to cool down the DAC to as low as 10 K; temperatures of the DAC were equilibrated after each cooling and were measured using two thermocouples attached to each side of the DAC. Temperature uncertainties were less than 5 K. SMS measurements with a resonant energy (E_0) of 14.4125 keV for ^{57}Fe were performed at the undulator beamline 16-IDD of the Advanced Photon Source (APS), Argonne National Laboratory (ANL). The energy band-width of the undulator beam was monochromotized to approximately 2 meV bandwidth using a water-cooled diamond (1 1 1) double crystal monochromator and a high resolution monochromator consisting of 2 channel cut silicon crystals (Si(4 4 0) and Si(9 7 5)). A pair of KB mirrors was used to focus the x-ray beam to approximately 50 μm at the sample position in the DAC. SMS spectra were collected using an avalanche photodiode detector at the nuclear forward scattering geometry with a collection time of 1–2 hours. SMS spectra were collected in the form of the intensity of the ^{57}Fe nuclear decay as a function of time. When the nuclei in the sample

are excited by the synchrotron radiation pulse of 14.4125 meV with a bandwidth of +1 meV, the coherent decay of the excited ensemble of nuclei phases with time. Through analyses of the time-resolved intensity of the SMS spectra, hyperfine parameters, including hyperfine magnetic fields, containing structural and electronic information of the resonating nucleus can be derived. The high resolution ($\Delta E/E \sim 1*10^{-7}$) of the SMS technique enables us to detect the AFM to PM phase transition of $SrFe_2As_2$ at high pressures. The spectra were fitted using the CONUSS program[35] to derive hyperfine parameters including hyperfine magnetic fields of the Fe ions.

Angle-dispersive XRD measurements were performed on powder samples at the 16-IDB beamline of the APS, ANL. The powder samples were gently ground from the same batch of the ^{57}Fe-enriched single crystals used for SMS experiments and loaded into the same symmetric DAC using Ne pressure medium and ruby pressure calibrate. XRD measurements of the starting sample showed consistent lattice parameters to the single crystals. To avoid systematic errors, care was taken to ensure that experimental conditions between SMS and XRD experiments were consistent: the same cryostat with the same temperature thermocouples and membrane controller were used in both experiments. Two types of XRD experiments were conducted: decreasing temperatures at a constant pressure with an x-ray wavelength of 0.4072 Å; increasing pressures at a constant temperature of 50 K or 13 K with an x-ray wavelength of 0.3737 Å. Diffraction patterns were collected by a MAR345 detector and processed using the FIT2D software. Rietveld refinements of the patterns were performed using the GSAS package[36].

1. Kamihara, Y., Watanabe, T., Hirano, M. & Hosono, H. Iron-based layered superconductor $La[O_{1-x}F_x]FeAs$ (x = 0.05–0.12) with T_c = 26 K. *J. Am. Chem. Soc.* **130**, 3296–3297 (2008).
2. Rotter, M., Tegel, M. & Johrendt, D. Superconductivity at 38 K in the iron arsenide $(Ba_{1-x}K_x)Fe_2As_2$. *Phys. Rev. Lett.* **101**, 107006 (2008).
3. Wang, X. C. *et al.* The superconductivity at 18 K in LiFeAs system. *Solid State Commun.* **148**, 538–540 (2008).
4. Hsu, F. C. *et al.* Superconductivity in the PbO-type structure α-FeSe. *Proc. Natl. Acad. Sci.* **105**, 14262–14264 (2008).
5. de la Cruz, C. *et al.* Magnetic order close to superconductivity in the iron-based layered $LaO_{1-x}F_xFeAs$ systems. *Nature* **453**, 899–902 (2008).
6. Huang, Q. Z. *et al.* Neutron-Diffraction measurement of magnetic order and a structural transition in the parent $BaFe_2As_2$ compound of FeAs-Based high temperature superconductors. *Phys. Rev. Lett.* **101**, 257003 (2008).
7. Paglione, J. & Green, R. L. High-temperature superconductivity in iron-based materials. *Nat. Phys.* **6**, 645–658 (2010).
8. Stewart, G. R. Superconductivity in iron compounds. *Rev. Mod. Phys.* **83**, 1589–1652 (2011).
9. Ishida, K., Nakai, Y. & Hosono, H. To what extent iron-pnictide new superconductors have been clarified: a progress report. *J. Phy. Soc. Jpn.* **78**, 062001 (2009).
10. Krellner, C. *et al.* Magnetic and structural transitions in layered iron arsenide systems: AFe_2As_2 versus RFeAsO. *Phys. Rev. B* **78**, 100504 (R) (2008).
11. Jesche, A. *et al.* Strong coupling between magnetic and structural order parameters in $SrFe_2As_2$. *Phys. Rev. B* **78**, 180504 (R) (2008).
12. Igawa, K. *et al.* Pressure-induced superconductivity in iron pnictide compound $SrFe_2As_2$. *J. Phys. Soc. Jpn.* **78**, 025001 (2009).
13. Sasmal, K. *et al.* Superconducting Fe-based compounds $(A_{1-x}Sr_x)Fe_2As_2$ with *A* = K and Cs with transition temperature up to 37 K. *Phys. Rev. Lett.* **101**, 107007 (2008).
14. Leithe-Jasper, A., Schnelle, W., Geibel, C. & Rosner, H. Superconducting state in $SrFe_{2-x}Co_xAs_2$ by internal doping of the iron arsenide layers. *Phys. Rev. Lett.* **101**, 207004 (2008).
15. Pratt, D. K. *et al.* Coexistence of competing antiferromagnetic and superconducting phases in the underdoped $Ba(Fe_{0.953}Co_{0.047})_2As_2$ compound using x-ray and neutron scattering techniques. *Phys. Rev. Lett.* **103**, 087001 (2009).
16. Park, J. T. *et al.* Electronic phase separation in the slightly underdoped iron pnictide superconductor $Ba_{1-x}K_xFe_2As_2$. *Phys. Rev. Lett.* **102**, 117006 (2009).
17. Chu, C. W. & Lorens, B. High pressure studies on Fe-Pnictide superconductors. *Physica C* **469**, 385–395 (2009).
18. Sefat, A. S. Pressure effects on two superconducting iron-based families. *Rep. Prog. Phys.* **74**, 124502 (2011).
19. Takahashi, H. *et al.* Superconductivity at 43 K in an iron-based layered compound $LaO_{1-x}F_xFeAs$. *Nature* **453**, 376–378 (2008).
20. Masaki, S. *et al.* Precise pressure dependence of the superconducting transition temperature of FeSe: Resistivity and ^{77}Se-NMR study. *J. Phys. Soc. Jpn.* **78**, 063704 (2009).
21. Zhang, S. J. *et al.* Effect of pressure on the iron arsenide superconductor Li_xFeAs (x = 0.8, 1.0, 1.1). *Phys. Rev. B* **80**, 014506 (2009).
22. Zhang, S. J. *et al.* Superconductivity at 31 K in the "111"-type iron arsenide superconductor $Na_{1-x}FeAs$ induced by pressure. *Europhys. Lett.* **88**, 47008 (2009).
23. Mydeen, K. *et al.* Temperature-presure phase diagram of the superconducting iron pnictide LiFeP. *Phys. Rev. B* **82**, 014514 (2010).
24. Ishikawa, F. *et al.* Zero-resistance superconducting phase in $BaFe_2As_2$ under high pressure. *Phys. Rev. B* **79**, 172506 (2009).
25. Matsubavashi, K. *et al.* Intrinsic properties of AFe_2As_2 (*A* = Ba, Sr) single crystal under highly hysrostatic pressure conditions. *J. Phys. Soc. Jpn.* **78**, 073706 (2009).
26. Colombier, E., Bud'ko, S. L., Ni, N. & Canfield, P. C. Complete pressure-dependent phase diagrams for $SrFe_2As_2$ and $BaFe_2As_2$. *Phys. Rev. B* **79**, 224518 (2009).
27. Torikachvili, M. S., Bud'ko, S. L., Ni, N. & Canfield, P. C. Pressure induced superconductivity in $CaFe_2As_2$. *Phys. Rev. Lett.* **101**, 057006 (2008).
28. Kotegawa, H., Sugawara, H., & Tou, H. Abrupt emergence of pressure-induced superconductivity of 34 K in $SrFe_2As_2$: A resistivity study under pressure. *J. Phys. Soc. Jpn.* **78**, 013709 (2009).
29. Kotegawa, H. *et al.* Effect of uniaxial stress for pressure-induced superconductor $SrFe_2As_2$. *J. Phys. Soc. Jpn.* **78**, 083702 (2009).
30. Yamazaki, T. *et al.* Appearance of pressure-induced superconductivity in $BaFe_2As_2$ under hydrostatic conditions and its extremely high sensitivity to uniaxial stress. *Phys. Rev. B* **81**, 224511 (2010).
31. Duncan, W. J. *et al.* High pressure study of $BaFe_2As_2$-the role of hydrostaticity and uniaxial stress. *J. Phys.: Condens. Matter* **22**, 052201 (2010).
32. Nakai, Y. *et al.* Unconventional superconductivity and antiferromagnetic quantum critical behavior in the isovalent-doped $BaFe_2(As_{1-x}P_x)_2$. *Phys. Rev. Lett.* **105**, 107003 (2010).
33. Zhou, R. *et al.* Quantum criticality in electron-doped $BaFe_{2-x}Ni_xAs_2$. *Nat. Lett.Commun.* **4**, 2265 (2013).
34. Wang, X. F. *et al.* Anisotropy in the electrical resistivity and susceptibility of superconducting $BaFe_2As_2$ single crystals. *Phys. Rev. Lett.* **102**, 117005 (2009).
35. Sturhahn, W. CONUSS and PHOENIX: Evaluation of nuclear resonant scattering data. *Hyperfine Interact.* **125**, 149–172 (2000).
36. Larson, A. C. & Von Dreele, R. B. *General Structure Analysis System (GSAS), Los Alamos National Laboratory Report* LAUR 86–748 (1994).

Acknowledgments

Work is supported by NFS and MOST of China through research projects. We appreciate C. Kenney-Benson for his assistance in setting up the cryogenic and online ruby systems at HPCAT. This work was performed at HPCAT (sector 16), Advanced Photon Source (APS), Argonne National Laboratory. HPCAT is supported by CIW, CDAC, UNLV and LLNL through funding from DOE-NNSA, DOE-BES and NFS. APS is supported by DOE-BES, under Contract No. DE-AC02-06CH11357. Work at UT Austin is supported by Energy Frontier Research in Extreme Environments (EFree).

Author contributions

C.Q.J. and J.F.L. conceived & designed the research; J.J.W., J.L.Z., X.C.W., Q.Q.L., Y.M.X. and P.C. conducted the experiments; J.J.W., J.F.L. and C.Q.J. wrote the paper.

Additional information

Competing financial interests: The authors declare no competing financial interests.

How to cite this article: Wu, J.J. *et al.* Magnetic and structural transitions of $SrFe_2As_2$ at high pressure and low temperature. *Sci. Rep.* **4**, 3685; DOI:10.1038/srep03685 (2014).